ASL Environmental Sciences Inc.
#1-6703 Rajpur Place
Saanichton, BC Canada V8M 1Z5
December, 30, 2022
TECHNICAL REPORT

The interpretation of multi-frequency acoustic profiling; Part 1, Exact solutions and their role in the evaluation of acoustic backscatter models.

David R. Topham[1] and J.R. Marko[1]
[1]ASL Environmental Sciences Inc., Saanichton, BC, Canada
Correspondence: David R. Topham (dtopham@aslenv.com)

Abstract

A set of multi-frequency acoustic equations, sufficient to describe a suspension in terms of a two parameter distribution function defined in terms of an equivalent volume sphere, is examined to determine the conditions necessary to deliver solutions for a given data set. For three incident acoustic frequencies, the equations are fully determined, and in principle, the solutions are exact. A criterion is developed to establish the existence of exact 3-frequency solutions directly from the data before analysis is undertaken. With access to four or more frequencies, comparison of alternative independent solutions provides a measure of the quality of the match between the backscatter model and the data, providing a powerful diagnostic tool. The methodology is illustrated by examples drawn from the elastic sphere as a backscatter model, with a frazil ice data set serving as an example of evaluation where the particle geometry differs maximally from the elastic sphere model.

1. Introduction

The use of near simultaneous sequences of high frequency acoustic pulses to establish the physical properties of populations of suspended matter is a long established technique in many fields, examples ranging from tracking sediment transport, to ocean surveys of suspensions of biomass. In most cases, the extraction of the physical properties of the target from the backscattered acoustic energy is well understood, and occupies an extensive body of literature; for example, Hay and Sheng, 1992, Crawford and Hay, 1993, Stanton et al. 1997. The more recent application of the technique to the formation of frazil ice in rivers, (Marko and Jasek, 2010, Marko et al. 2015, Marko and Topham, 2021, McFarlane et al. 2017), and in the vicinity of Antarctic ice shelves (Frazer et al. 2020, Kungl et al. 2020), is less well developed, with questions arising as to the acoustic scattering properties of the disk shaped ice particles.

Here, the fundamental question is explored of the conditions necessary for a theoretical acoustic backscatter model to yield solutions for a given multi-frequency data set. Specifically, criteria are developed for a theoretical model with a two parameter particle distribution to deliver valid solutions for given multi-frequency data set. For three sampling frequencies, the set of equations is fully determined and in principle, the solutions are exact. In this context, the term exact refers to the computational precision of the algorithm, not to the physical properties of the target suspension. This requires additional acoustic frequencies to provide alternative sets of three

frequency combinations, each enclosing a different range of the model backscatter relationship. This generates a set of independent, high precision solutions for the same physical target; their inter-comparison then provides a measure of the accuracy of the physical property estimates. The significance of the existence criteria is that they enable the existence of valid 3-frequency solutions to be established for a data set prior to analysis. The high precision of the solutions serves as an identifier, providing confirmation that the algorithm is functioning as intended; it is of negligible consequence in the context of the final estimates of the physical properties of the target suspension.

.

2.0 Basic theory of measurements and extraction/characterization procedures.

The analysis is subject to the following assumptions:

1. That the total flux of backscattered acoustic energy is the sum of the energy scattered by individual particles.
2. That the normalized particle backscatter cross section, $\sigma_{BS}/\pi\hat{a}^2$ is a unique function of the parameter $k_1\hat{a}$, where the wave number k_1 is the incident acoustic wavelength, and $\hat{a}$ the characteristic length scale of an individual particle.

The general length scale $\hat{a}$ is taken here to be a_e , the radius of an equivalent volume sphere, Ashton (1983), a reflection of the inherent dependence of the physical scattering on target volume.

Data is specified in terms of volume backscatter coefficients, $s_V(v_i)$, defined as the scattered fraction of acoustic power incident on a unit volume suspension. at frequency, v_i. In general terms, the backscattered energy balance for measurements made in each of n different frequency channels can be expressed as:

$$s_V(v_i)=N\int_0^\infty g(a_e)\sigma_{BS}(a_e,v_i)da_e \quad , \tag{1}$$

where N denotes the total number of particles per unit volume; $\boldsymbol{\sigma_{BS}}(\underline{a_e,v_i})$ the theoretical backscatter cross section of an individual particle at an acoustic frequency v_i, and a_e, the "effective sphere" radius. The parameter $\boldsymbol{\sigma_{BS}}(\underline{a_e,v_i})$ is distributed according to a two parameter probability distribution, $g(a_e)$, satisfying:

$$\int_0^\infty g(a_e)da_e=1 \tag{2}$$

For present purposes, a lognormal distribution function is assumed, Crawford and Hay (1993) for sediment transport, or for frazil ice, (Clark and Doering, 2006; McFarlane et al., 2015). The two parameter lognormal distribution:

$$g(a_e,a_m,b) = [(2\pi)^{0.5}ba_e]^{-1}e^{-0.5\left(\frac{ln(a_e/a_m)}{b}\right)^2} \quad , \tag{3}$$

is adopted for the computations. The descriptive population parameters are the mean effective radius, a_m, and b, the standard deviation of the natural logarithm of a_e which describes the "spread" in effective radius values.

The particle number density N appears as a common multiplying factor in the set of equations (1), and can be eliminated by division to express the equations in terms of ratios of backscatter coefficients (Hay and Sheng, 1992), denoted by $G(i,j)$, where the indices i and j identify the individual data channels, ie. $G(2,1) \equiv s_V(\nu_2)/s_V(\nu_1)$, etc. This expands the set of n equations (1) to the number of possible combinations of (n-1) frequency pairs (i, j), ie. n!/(2(n-2)! equations of the form:

$$G(i,j)^{meas} = G(i,j) \tag{4}$$

$G(i,j)$ being the ratio of the right hand member of the set of equations (1).

For pairs of ratios sharing a common frequency, the equations (4) are fully determined, and in principle provide a computationally exact solution for the distribution parameters. The number density N then follows from the measured $s_V(\nu_i)$ values via equations (1).

The corresponding estimates of fractional volume F follow from,

$$F = N \int_0^\infty \left(\frac{4\pi}{3}\right) g(a_e, a_m, b) {a_e}^3 \, da_e \tag{5}$$

Considering just two frequencies reduces the problem to the less informative, but more widely applicable, two-channel analysis previously used by Marko and Jasek (2010). This limits the characterization of suspensions to the reduced parameters a^* and N^*, representing the target as a suspension of uniformly sized particles. The set of Eqns. (4) then reduces to a single equation in a^* for each of the independent G(i,j) ratios, where the volume backscatter coefficient equation simplifies to

$$s_V(\nu_i) = N^* \sigma_{BS}(a^*, \nu_i), \tag{6}$$

This representation does not realistically describe the details of the target suspension, but the inherent dependence of the physical scattering on target volume results in a relatively robust estimate of the fractional volume parameter F^*, where:

$$F^* = \frac{4\pi}{3} N^* {a^*}^3 \quad . \tag{7}$$

For a suitably narrow particle distributions, F^* is a good approximation to F.

The exact solutions can be identified from a simple least squares routine as vanishingly small values of the residual Q, defined by the sum of the squares of the residuals of the ratio equations,

$$Q = \sum_1^m [G(i,j)^{meas} - G(i,j)]^2 \tag{8}$$

where m = 1 for 2- frequency, and 2 for 3-frequency solutions respectively.

Ideally, the values of N returned by individual frequencies have identical values, their differences providing a further measure of the numerical precision of the solution.

2.1 The characteristics of the exact solutions.

The general structure of the exact solutions for the set of ratio equations (4), is discussed in a graphical framework, illustrated here for the elastic sphere, (Faran, 1951) and complimented by examples of data drawn from the 2011-12 Peace River 4-frequency frazil ice deployment of Marko et al. (2015). Specific examples are computed from the modern formulation of the sphere cross-section algorithm, publicly available as implemented by Dezhang Chu of the Northwest Fisheries Science Center). Data were acquired at, 125 kHz, 200 kHz, 455 kHz and 774 kHz respectively. Erratic behaviour of the 200 kHz channel 2 data, limited examples to just three channels, providing access to three, independent 2-channel solutions, and one 3-channel solution. To facilitate later discussion of this data, the backscatter ratios are referenced by combinations of the channel numbers 1, 3 and 4. For reference, the normalized backscatter cross section for an elastic sphere suspended in fresh water is shown in Fig 1; the symbols mark modifications arising from the discussion of Section 3.

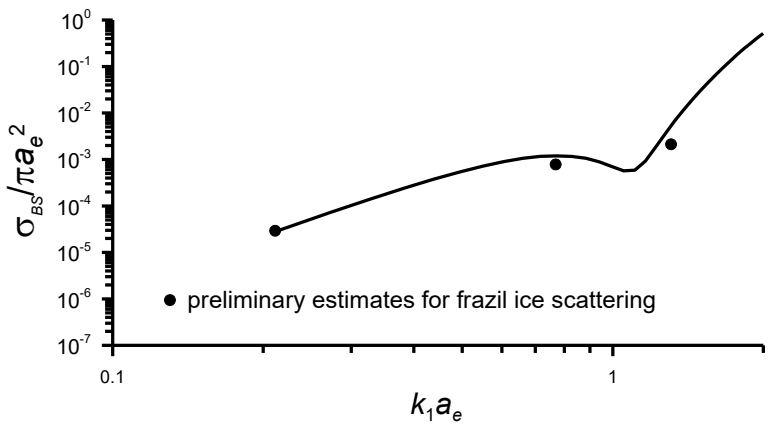

Figure 1. The normalized backscatter cross section for an elastic sphere of ice suspended in freshwater. Symbols indicate possible modifications deduced from disk shaped frazil ice scatterers.

2. 1.1 Two-channel solutions.

Each of the channel pairings, expressed in terms of the backscatter ratios provides an independent description of the physical parameters of the target, as shown Fig. 2. Solutions are determined by the intersections of the data, represented by the horizontal lines, with the corresponding theoretical functions. The particle number density N^* and fractional volume F^* then follow from equations (6) and (7). The existence of a solution only requires that the data is enclosed by the bounds of the appropriate branch of the $G(i,j)$ function. The data examples are drawn from the Peace River data of Table 2, Section 3.

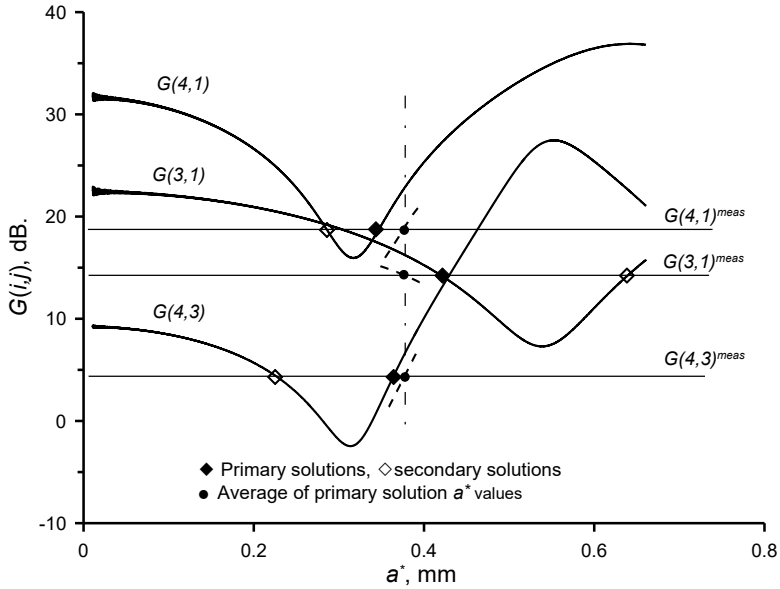

Figure 2. Illustration of two-frequency solutions obtained from intersections, denoted by diamond-shaped markers. of measured (4,1), (3,1) and (4,3) backscatter coefficient ratios (light horizontal lines) with corresponding theoretical functions. The vertical broken line marks the mean value of a^* at 0.38 mm. The displaced dashed segments of the curves relate to the discussion of Section 3.

The *G(i,j)* functions are two-valued within the range of interest, with solutions marked by diamond symbols, and designated as "lower" and "upper" branch solutions with respect to the function minima. The physically relevant solutions for the three channel combinations, marked by solid diamonds, represent the same physical target, and their dispersion about the mean value, marked by the chain dotted line, is a measure of the overall accuracy. The secondary solutions, marked by open symbols, are more widely dispersed, and, in this example, are easily distinguished. For solutions occurring close to the function minima, the correct choice of solution can be problematic. This ambiguity is resolved by consideration of the three-channel solutions.

2.1.2 Three channel solutions

For the more informative three-channel solutions, two measured backscatter ratios must share a common solution for both a_m and b. The structure of the solutions is illustrated in Fig. 3 for the (3,1) and (4,3) channel combinations as full and dashed lines respectively, identified by the particle distribution parameter b. The two horizontal lines represent the measured input ratios for a hypothetical input data point having the solution a_m = 0.274 mm, and b=0.2, (marked by solid symbols). Note that the second intersection of the data with the lower branch of the *G(4,3)* curves at a lower a_m have no matching *G(3,1)* intersection, establishing that the three-channel solutions are single valued, and confined to the upper branch of the *G(4,3)* curve. As in the two-frequency case, the number density parameter N is then calculated from the solution and in combination with a measured backscatter coefficient, substituted in Eq.1; the fractional volume, F following from Eqn. 5.

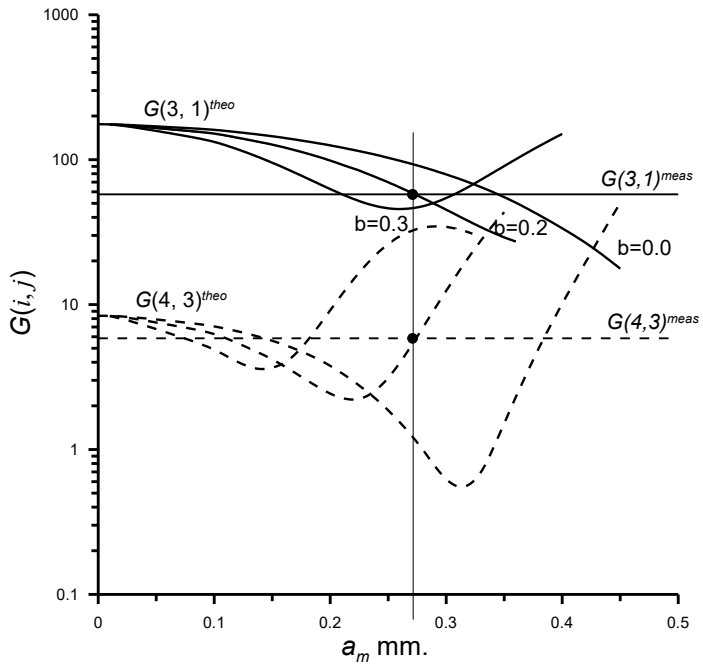

Figure 3. A graphical illustration of a three-channel solution using the (3,1) and (4,3) pairs. The solution space is specific to the elastic sphere model.

In the limit as b approaches zero, the branch pairings define the branch of corresponding two-channel solutions for each included channel pair, resolving the previously noted the two-channel ambiguity. The branch pairings of the *G(i,j)* functions for the possible three-channel combinations are listed in Table 1. Each pairing contains the same frequency information, and thus represents the same solution. The solution branches are unique to the individual channel pairs and hence define the relevant branches of the corresponding two-channel solutions.

Table 1. Branch pair combinations for the 3-channel elastic sphere solutions.

Branch pair combinations	
G(4,1) Upper	*G(4,3)* Upper
G(3,1) Lower	*G(4,3)* Upper
G(3,1) Lower	*G(4,1)* Upper

Each value of a_m defines a pair of boundary points on Fig. 3 enclosing a range of input data capable of supporting three-channel solutions; the upper and lower boundaries respectively defined by the $G(3,1)_{b=0}$ curve, and the upper branch of the $G(4,3)_{b=0}$ curve, (corresponding equivalent boundaries can be defined for the alternative channel pairings listed in Table 1). The relationship between these boundary values establishes the necessary condition to be satisfied by the data for the existence of the three-channel solutions. Solutions for particular values of b are further constrained to a_m values between the minimum of the *G(4,3)* function and its intersection with the *G(3,1)* function,. Where the functions fail to intersect, as illustrated for $b = 0.3$, solutions are limited by the minimum of the *G(3,1)* function.

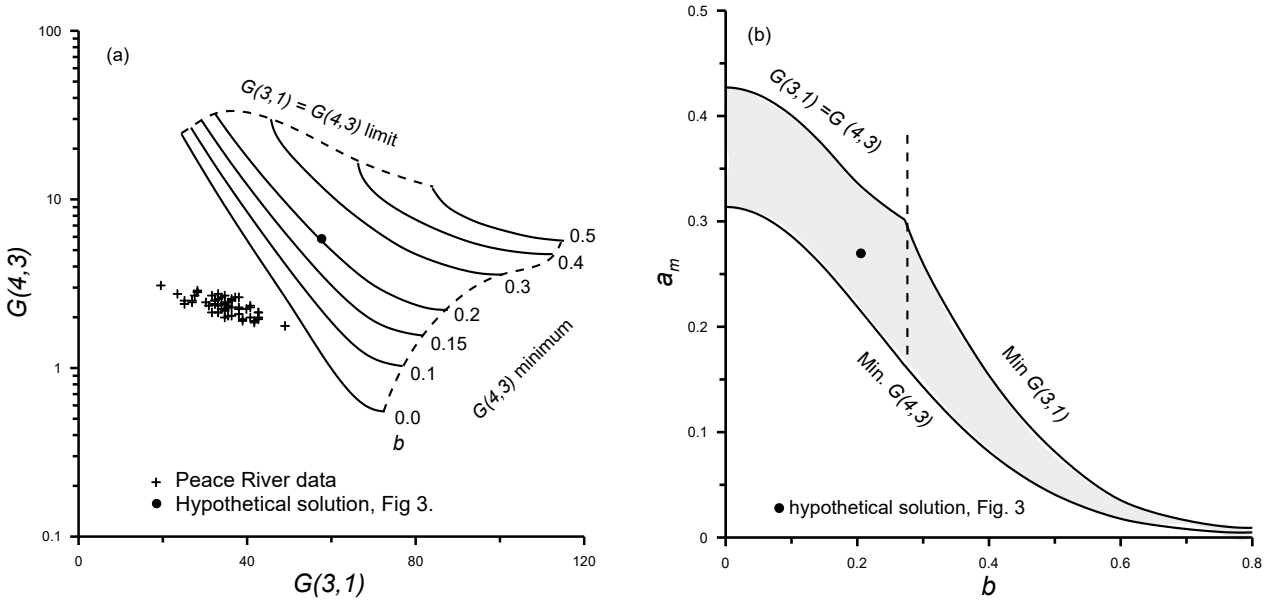

Figure 4. (a) The existence diagram for elastic sphere 3-frequency solutions, + data points for Peace River frazil ice; (b) The solution map for the elastic sphere.

Fig. (4a) shows the existence diagram for 3-channel solutions of the elastic sphere *G(3,1)* and *G(4,3)* pairing, the thicker line indicating the critical *b*=0 boundary, the data points of the March 20 Peace River frazil interval demonstrate that no 3-channel solutions exist for this data set when analysed with the elastic sphere model. Figure 4b maps the corresponding parameter boundaries in (b, a_m) space. In cases where solutions exist, appropriate initial values of a_m and b must be assigned to ensure convergence to the exact solution. Ideally, these should lie within the shaded area of Fig 4b, a suitable value of b being available from Fig. 4a. For the elastic sphere illustrated here, initial conditions below the lower boundary of Fig 4b also converge. In the case where a 3-channel solution is sought where none exist, the search algorithm progresses to a state with b≈0, returning value of a_m approximating the mean of the three possible individual 2-channel solutions.

3.0 Evaluation of the elastic sphere for the representation of non-spherical acoustic targets.

The availability of a set of multi-frequency acoustic profiling data of frazil ice suspensions provides the opportunity to evaluate the application of the equivalent volume elastic sphere for analysis of weakly buoyant suspensions of disk-shaped particles. The analysis was carried out on 2-minute averaged Peace River s_V data from a 20 March, 2012 time interval representative of the most commonly occurring "single-peak" form of frazil interval, usually associated with moderate supercooling conditions (Marko et al., 2015). The existence criteria have established that no three-channel solutions can be found for this analysis, Fig. 4a . The evaluation, therefore, is confined to two-frequency analysis under the assumption of a uniform particle distribution of radius a^*. The loss of data channel 2 limited the evaluation to three independent 2-frequency solutions. The validations are based on the relatively robust estimates of derived frazil fractional volumes.

,

The full time series of F^* for the two-channel pairings: (3,1), (4,3) and (4,1) are shown in Figs. 5a, b and c. Panels (a) and (b) are similar, with somewhat lower peak values for the latter case. Panel (c), representing results in which the channel pairing is separated by the full frequency range, has a more prominent peak and, overall, a notably exaggerated scatter.

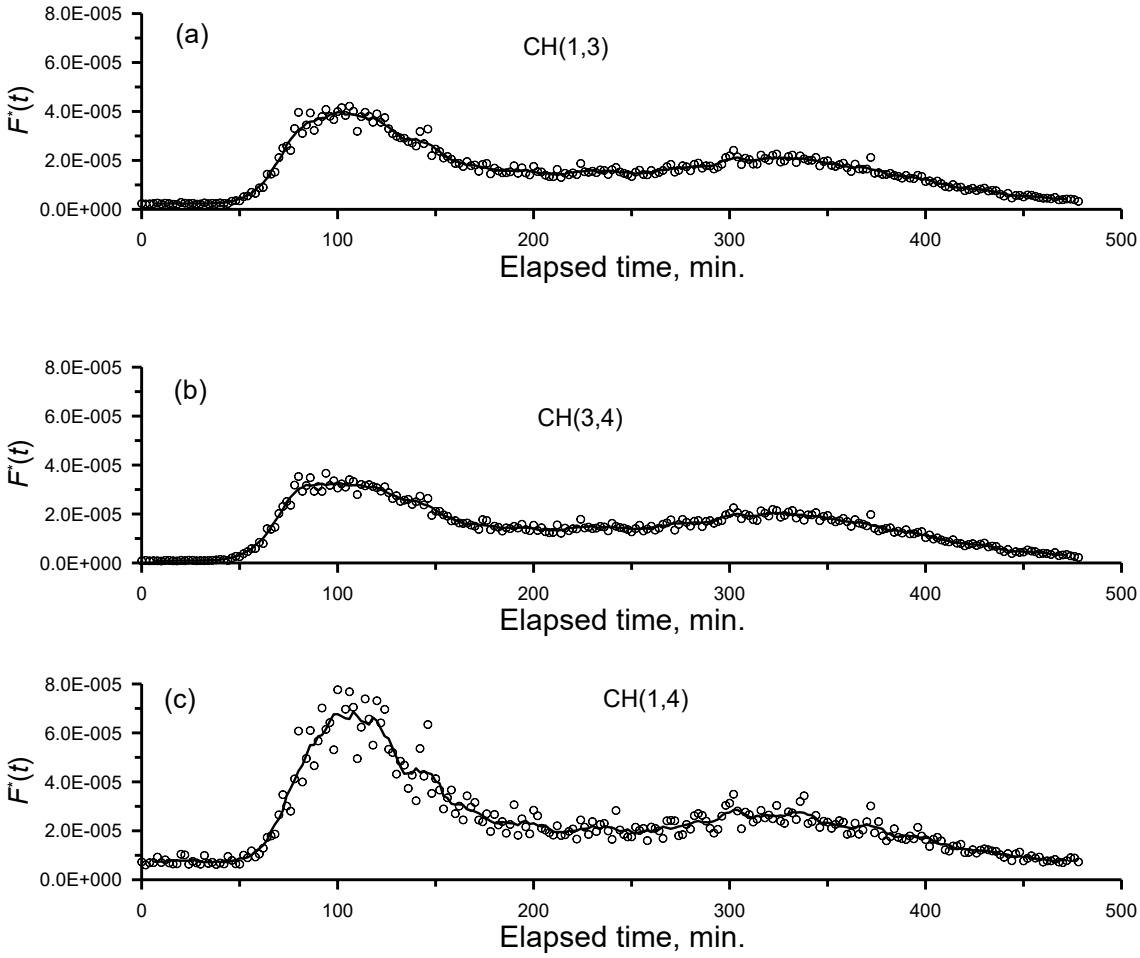

Figure 5. Comparisons of the March 20 frazil fractional volume as derived with the data channel combinations: (a), (3,1); (b), (4,1) and (c), (4,3).

Detailed quantitative comparisons focus on average values over the 90-110 minute interval encompassing the peak fractional volumes. Key results and relevant parameters deduced for this period are summarized in the first three rows of Table 2 for the available channel pairings. Listed values are overall averages of two-channel extractions from ten individual data points and are equivalent to a single time averaged data set centred on the peak of the curves of Fig.5.

Table 2. Results of the three possible two-channel extractions from s_v data.

Channels	Peak a_e^*	Peak F^*(t)	Peak N^*(t)	$F^*(t)/F^*_{Mean}$	Lowest value of $k_1a_e^*$ or k_1a_m	Highest value of $k_1a_e^*$ or k_1a_m
3,1 (lower)	0.420	3.85E-05	1.24E+05	0.847	0.235	0.856
4,3 (upper)	0.365	3.15E-05	1.55E+05	0.694	0.744	1.265
4,1 (upper)	0.346	6.63E-05	3.82E+05	1.46	0.194	1.200
Means	0.377	4.54E-05	2.20E+05	1	n/a	n/a

The entries in the first column specify pair composition and the relevant branch of the corresponding *G(i,j)* curve. The final two columns list values of k_1a_e corresponding to the lowest and highest acoustic frequency associated with each extraction. The opposing effects of changes in a_e^* and N^* allow relatively robust estimates of the fractional volume, F^*, which reflect the dominant role of target volume in the scattering response of the weakly buoyant suspensions.

The F^* values for the (3,1) and (4,3) pairs, differ by 20%, an encouraging result, given that the joint k_1a_e range embraces the local minimum of the sphere cross section characteristic. For the (4,1) pair, spanning the upper and lower k_1a_e extremes, the F^* value exceeds the (3,1) and (4,3) pair values by a factor of roughly 2.

The spread in a_e^* values is illustrated in Fig 2 in the graphical representation of the solutions, with the vertical chain-dotted line marking the overall average a_e^* value and small circular symbols marking intersections with the corresponding data inputs. Assuming the channel-averaged value of a^* as a plausible solution for a hypothetical, fully self-consistent (i.e. channel-independent) extraction algorithm, requires modified *G(i,j)* functions which satisfy the input data at the channel-averaged a^* values, illustrated by the short downward shifted dashed line segments. This places the data point on the critical boundary of a modified *G(3,1)*, *G(4,3)* existence map. Assuming that k_1a_e values associated with channel 1 data are sufficiently low to be represented by the elastic sphere model, the downward shifts in the *G(i,j)* functions translate into corresponding shifts in the normalized cross section characteristic, indicated by the solid points on Figure 1. These suggested modifications are consistent with laboratory measurements on polystyrene disks and spheres, Marko and Topham, (2015).

4.0 Summary and conclusions

A set of multi-frequency acoustic equations, sufficient to describe a suspension in terms of a two parameter distribution function defined in terms of an equivalent volume sphere, is examined to determine the conditions necessary to deliver solutions for a given data set. Of primary interest is the accuracy of estimates of suspended fractional volumes. For three incident acoustic frequencies, the equations are fully determined, and in principle, the solutions are exact. In order to realise the exact solutions, it is necessary to express the equations in terms of ratios of volume backscatter coefficients, (Hay and Shen, 1992). This reduces the problem to a pair of equations in the particle distribution parameters, with a subsequent calculation of particle number density utilizing the measured volume backscatter coefficients. A relationship between the theoretical backscatter

ratios defines the criterion which must be satisfied by the corresponding measured ratios for the existence of exact solutions. This allows the existence of 3-frequency solutions to be established directly from the data before a full analysis is attempted.

In this context, the term "exact" refers to the numerical precision of the algorithm, not to the accuracy of the representation of the physical acoustic target. To establish accuracy additional frequencies are required to generate alternative pairs of ratios sharing a common frequency, each providing an, independent, 3-frequency solution for the same acoustic target. Inter-comparisons of these independent solutions then provide a measure of the quality of the match between the theoretical backscatter model and the data. In this respect. evaluation is greatly enhanced by the inclusion of the more accessible, but less informative, 2-frequency solutions based on a uniform particle distribution. Where 3-frequency solutions are not available, the 2-frequency solutions provide relatively robust estimates of fractional volumes.

For more than three frequencies, the number of data ratios increases factorially, with pairs of ratios sharing a common frequency providing additional, independent, 3-frequency solutions for the same acoustic target. The inter-comparison of these independent solutions then provides a measure of the quality of the match between the theoretical backscatter model and the data. In a practical application with a fully validated scattering model, the existence criterion acts as a pre-analysis filter to locate inappropriate data points. Conversely, as in the example included here, the data can be applied to assess the performance of the algorithm. The high precision of the exact solutions is insignificant in the context of the overall error estimates, it provides confirmation that the correct solution has been returned. The high precision eliminates uncertainties associated with the convergence of the algorithm from error estimates.

The general methodology is illustrated throughout by results drawn from the elastic sphere as an example of a theoretical model. The evaluation procedure is demonstrated by the application of the elastic sphere model to a frazil ice data set, a case where the thin disk geometry differs maximumly from the spherical geometry of the model. The existence criterion establishes that while the elastic sphere model cannot provide the 3-frequency solutions, validation based on the 2-frequency analysis suggests modifications to the spherical backscatter model sufficient to satisfy the 3-frequency existence criterion. These modifications, shown in Fig 1, are consistent with laboratory measurements on polystyrene disks and spheres, Marko and Topham, (2015).

References

Ashton, G. D., 1983: Frazil ice. In: Theory of Dispersed Multiphase Flow, Academic Press N.Y., 271-289.

Chu, D., Northwest Fisheries Science Center. (https://bitbucket.org/gjm/calibration-code/wiki/Home).

Clark, S., Doering, J. 2006: Laboratory Experiments on Frazil Size Characterizations in a Counterrotating Flume, J. Hydraulic Engineering, pp, 94-101.

Crawford, A. M. and Hay, A. E., 1993: Determining suspended sand size and concentration from multifrequency acoustic backscatter. J. Acoust. Soc. Am. 94 (6) pp. 3312-3324.

Faran, J.J. Jr., 1951: Sound scattering by solid cylinders and spheres. J. Acoust. Soc. 23, pp 405-418.

Frazer, E. K., Langhorne, P. J, Leonard, G. H., Robinson, N.J. and Dániel Schumayer, D. Observations of the size distribution of frazil ice in an ice shelf water plume., 2020. Geophy. Res. Letters, 47, e2020GL090498, https://doi.org/10.1029/2020GL09049.

Hay, A. E, and Sheng, J. 1992: Vertical profiles of suspended sand concentrations and size from multifrequency acoustic backscatter. J. Geophys. Res. 97 (10), pp 1566-1567.

Kungl, A. F., Schumayer, D., Eamon K. Frazer, A. K., Pat J. Langhorn, P. J., Greg, H., Leonard, G. H., 2020: An oblate spheroidal model for multi-frequency acoustic back-scattering of frazil ice. Cold Reg. Sci Technol, 177, https://doi.org/10.1016/103122.

Marko, J.R., Jasek, M., 2010: Frazil monitoring by multi-frequency shallow water ice profiling (SWIPSA): present state. Proc. IAHR 20th International Symposium on Ice, Lahti, Finland. 12p.

Marko, J.R., Jasek, M., Topham, D.R., 2015: Multifrequency Analyses of 2011-2012 Peace River SWIPS frazil backscattering data. Cold Reg. Sci. Technol. 110, 102-119.

Marko, J.R., Topham, D.R., 2021: Analyses of Peace River shallow water ice profiling sonar data and their implications for the roles played by frazil ice and in situ anchor ice growth in a freezing river. The Cryosphere 15, 2473-2489, https://doi. Org/10.5194/tc-13-2473.

McFarlane, V., Loewen, M., Hicks, F., 2017: Measurements of the size distributions of frazil ice particles in three Alberta rivers. Cold Reg. Sci. Technol. 142, pp. 100-117,

Stanton, T.K, Wiebe, P.H., Chu, D., 1998: Differences between sound scattering by weakly scattering spheres and finite-length cylinders with applications to sound scattering by zooplankton. J. Acoust. Soc. Am. 103 (1) 1998.